VOL. 14, NO. 5 J. SPACECRAFT MAY 1977

Numerical Computations of Orbiter Flowfields and Laminar Heating Rates

W. D. Goodrich*
NASA Lyndon B. Johnson Space Center, Houston, Texas
and
C. P. Li,† C. K. Houston,† P. B. Chiu,‡ and L. Olmedo§
Lockheed Electronics Company, Inc., Houston, Texas

Numerical computations of flowfields and laminar heating rates around the Space Shuttle Orbiter windward surface, including the root of the wing leading edge, are presented to illustrate the sensitivity of these calculations to several flowfield modeling assumptions. Specifically, results obtained using the axisymmetric analogue concept to predict "three-dimensional" heating rates, in conjunction with exact three-dimensional inviscid flowfield solutions and two-dimensional boundary-layer analysis, show the sensitivity of boundary-layer edge conditions and heating rates to considerations of: 1) the inviscid flowfield "entropy layer," 2) equilibrium air vs chemically and vibrationally frozen flow, and 3) nonsimilar terms in the boundary-layer computations. In addition, a cursory comparison between flowfield predictions (made at critical points in the current design trajectory) obtained from these methods and current Orbiter design methods has established a benchmark for selecting and adjusting these and future design methodologies.

Nomenclature

B = Orbiter half-span, see Fig. 1
F = ratio of 3-D to axisymmetric stagnation point heating, see Eq. (4)
h = inviscid surface streamline metric, enthalpy
h_{aw} = adiabatic wall recovery enthalpy
K = ratio of principal velocity gradients at the stagnation point, see Eq. (3)
L = Orbiter length, see Fig. 1
M = Mach number
p = pressure, atm
q = heat transfer rate, BTU/ft^2-sec
R_n = nose-cap radius, see Fig. 1
Re_x = Reynolds number based on axial distance, x
s,n = surface streamline coordinates
T_w = wall temperature, °R
u,w = streamwise and crossflow velocities
V_∞ = freestream velocity, ft/sec
x,r,ϕ = cylindrical coordinates
x,y,z = Cartesian coordinates
β = boundary-layer pressure gradient parameter $= 2(d\ell n\, u_e/d\ell n\, \xi)$
δ = boundary-layer thickness, ft
γ = specific heat ratio
θ = boundary-layer momentum thickness, ft
μ = viscosity
ξ = transformed surface streamline coordinate $= \int_0^x \rho_w \mu_w u_e h\, dx$
ρ = density

Subscripts

e = refers to conditions at boundary-layer edge
δ = edge conditions determined at δ in flowfield
0 = edge conditions determined using surface pressure and normal-shock entropy, axisymmetric stagnation point
s = 3-D stagnation point

Introduction

As part of the final testing and certification of the Space Shuttle transportation system, the first Shuttle launch and entry (Orbiter) system will undergo orbital flight testing in early 1979. Part of this flight test program will be focused on providing data to certify the Orbiter heat shield, or thermal protection system (TPS) design, and its heating environment during hypersonic entry. Quite naturally, as in past NASA manned orbital entry programs, wind-tunnel testing has played a major role in establishing the aerothermodynamic environment necessary to design the TPS and to help define trajectories and operational constraints for the entry vehicle. However, unlike previous programs, flight performance and design objectives, which dictate the reuse of major system components (including the Orbiter for up to 100 missions) have required a nonconservative design philosophy which, in turn, has demanded a better understanding of the technologies which help design these systems. Specifically, the aerothermodynamic environment experienced by the Orbiter during entry, particularly the heat transfer rates and distribution, strongly influence vehicle structural design and TPS material selection, insulation thickness, and resultant system weight. Therefore, a better understanding of the factors which affect the Orbiter heating environment will help reduce potential uncertainties in the TPS design and anticipated performance. Since wind-tunnel testing alone cannot completely simulate the Orbiter entry environment, complimentary analyses and numerical flowfield computations are needed for a more complete Orbiter flowfield simulation.

The use of advanced three-dimensional (3-D) flowfield simulation methods as a means of providing more insight into the use of wind-tunnel data for making aerothermodynamic predictions at flight conditions was advanced by Goodrich et al[1] in 1975. In that study, conventional design methods based

---

Received July 1, 1976; presented as Paper 76-359 at the AIAA 9th Fluid and Plasma Dynamics Conference, San Diego, Calif., July 14-16, 1976; revision received Nov. 15, 1976.

Index categories: Boundary Layer and Convective Heat Transfer—Laminar; Supersonic and Hypersonic Flow.

*Senior Engineer, Structures and Mechanics Division. Member AIAA.

†Staff Engineer, Applied Mechanics Department. Member AIAA.

‡Principal Engineer, Applied Mechanics Department. Member AIAA.

§Computer Programming Analyst, Applied Mechanics Department.

on two-dimensional (2-D) flowfields (sphere, wedge, cone, etc.) and heating methods, which were calibrated or "three-dimensionalized" with wind-tunnel data, were compared to 3-D flowfield predictions of the Orbiter aerothermodynamic environment at a single hypersonic flight point. The major short-coming discovered in these conventional 2-D flowfield methods was the inability to accurately account for changes in heating and boundary-layer edge conditions caused by relative differences in the influence of the inviscid entropy layer at wind-tunnel and flight conditions.

In an effort to gain further insight into this effect and to identify the range of flight conditions where this effect may be important, the present study considered four flight points, taken from the current Orbiter design trajectory during the times of peak laminar heating and the beginning of boundary-layer transition. These conditions, which are shown in Table 1, provide rather significant changes in both the freestream flow conditions and the angles of attack. Because of these high-enthalpy flight conditions and angles of attack, an assessment of the influence of gas chemistry, and to some degree boundary-layer computational procedures in high-velocity gradient regions on the flowfield results, was desirable. Therefore, the general objective of this study was to examine the sensitivity of the Orbiter heating rates and boundary-layer edge conditions to considerations of: 1) the inviscid flowfield "entropy layer," 2) equilibrium air versus chemically and vibrationally frozen flow, and 3) nonsimilar terms in the boundary-layer computations. Direct comparisons with the tangent-cone based extrapolations of Orbiter wind-tunnel data, taken from the Orbiter design data book[2] at these four flight conditions, were also made. These comparisons may help to either verify the current design methods, or to identify areas where the current design environment can be improved.

Approach and Analysis

As indicated in the Introduction, "entropy-layer swallowing" (i.e., the process of ingesting the bow-shock-induced layer of high-entropy inviscid flow near the Orbiter surface by the boundary layer as it grows in going downstream from the stagnation point) plays a dominant role in establishing boundary-layer edge conditions and heating at flight conditions. This effect was shown in Ref. 1 to have a negligible influence on the Orbiter heating at wind-tunnel conditions, but was shown to be far more significant at flight conditions.

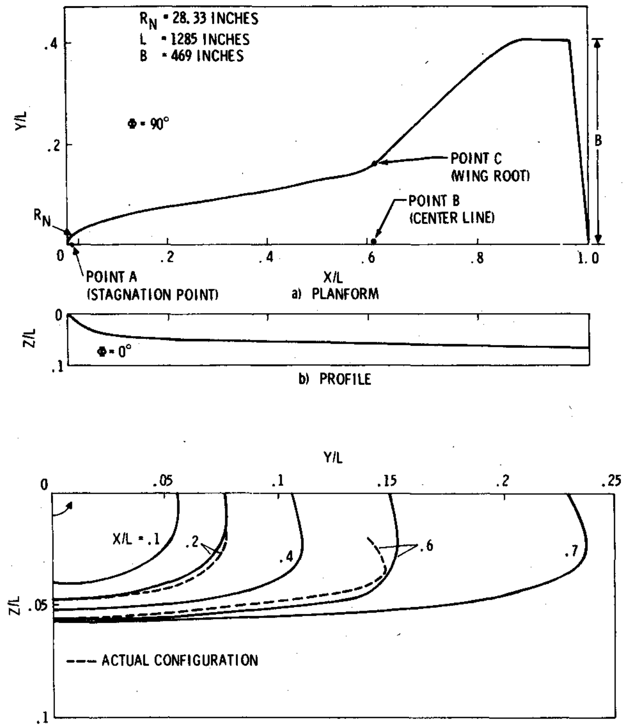

a) PLANFORM

b) PROFILE

c) CROSS SECTIONS

Fig. 1 Orbiter geometry.

Pursuant to the objectives described in the Introduction, results were generated for both normal-shock-entropy and local inviscid entropy edge conditions (established in the inviscid flow through an approximate means which considered the growth of the boundary layer into the inviscid flow) to illustrate the sensitivity of the boundary-layer results to changes in entropy edge conditions. To assess the effects of finite-rate-chemistry on the flowfield results, both equilibrium air and chemically and vibrationally frozen (a perfect gas with $\gamma = 1.4$) flowfields were computed. (These flowfields are limiting cases of finite-rate-chemistry flowfields.) In addition, comparisons were made between heating predictions obtained from sophisticated nonsimilar boundary-layer codes and simpler similarity-based heating correlations in an effort to assess the need for using the more complex procedures.

An assessment of the accuracy of these computer codes was made in Ref. 1 through comparisons with wind-tunnel data,[3,4] and more recently, through comparisons with the analyses of Refs. 5 and 6. Very basic information concerning the codes used for the current study, as well as specific analyses required to supplement thse codes, will be described in the following sections. However, detailed aspects of most of these codes and analyses will not be made since these descriptions are well documented in the cited references.

Flowfield and Boundary-Layer Codes

The numerical codes used for computing inviscid flowfields and heating rates to the Orbiter consists of several numerical procedures developed independently by numerous researchers. A significant part of the present work was devoted to establishing means of coupling these procedures and to implementing modifications to the existing programs when necessary.

To provide a relatively economical description of the complete Orbiter flowfield, inviscid/boundary-layer computations were employed, since spatial resolution requirements, and therefore computer time and size, were minimized. In this "two-layer" approach, local inviscid flow conditions were used to establish surface streamlines and local edge conditions necessary for making boundary-layer computations. Specifically, an inviscid version of the 3-D time-dependent code developed by Li[7] was used to start, or initialize, the inviscid codes developed by Kutler et al.[8,9] for integrating the 3-D steady-state Euler equations. Results from these flowfields were used to calculate surface streamlines and metric coefficients as outlined by Rakich and Meteer.[10] The 2-D boundary-layer solution procedure described by Tong et al.[11] was adopted as a "standard" for making predictions of surface heating and shear stress along these streamlines. This application of 2-D boundary-layer techniques to 3-D flow situations relies on the axisymmetric analogue concept which has been outlined by DeJarnette and Davis.[12] After extensive comparisons (at both wind-tunnel and flight conditions) of heating results obtained using several simple heating methods and the "standard" boundary-layer calculations, a "production" heat transfer prediction method was adopted to help save computer time and cost. Thus far, this simplified method, based on the development of Kemp et al,[13] has produced surface heating at both wind-tunnel and flight conditions to within five percent of the "standard" results.

Orbiter Geometry

The Orbiter geometry used for making these 3-D flowfield computations is shown in Fig. 1. Geometry data from the Rockwell 140-B Orbiter configuration was used to "gauge" or calibrate the analytical description of the Orbiter. Details of data requirements and analytical curves used for this procedure are presented in Ref. 8. Reasonably fine details of the basic geometric characteristics, suitable for making flowfield computations, were maintained on the windward surface, as shown by the cross-sectional comparison in Fig. 1c. These cross sections were formed by fitting single ellipses through control points located on the centerline and the "chine," or leading edge. Cubic functions and additional ellipses were used from the chine to the leeside pitch-plane. Control points on the windward pitch-plane and the meridional planes containing the chine were taken directly from design drawings. In the axial direction, a spline curve-fit procedure was used to insure continuity of the surface slopes. Note that the actual geometry near the beginning of the leeside was not simulated accurately, since the primary concern was to emphasize the flow surrounding the windward surface. Previous studies[1] have indicated that very little differences occur in the flowfield results obtained with different analytical curves representing the leeside geometry.

A drawing of the Orbiter planform, profile, and several cross sections are shown in Fig. 1. Note that the analytical curves are not as flat (have smaller cross-sectional radii of curvature near the nose centerline) as the real configuration. Note also that the fuselage leading edge, or chine, as well as the wing leading edge, are not as sharp. A better analytical representation of the chine and wing was used initially. However, this geometry produced rapidly varying slopes near the leading edges and could not be used with the current inviscid flowfield codes.

Streamline Metric

The metric coefficients, h, for the streamline coordinates, are used to describe the streamline divergence on the basis of the inviscid velocity field. Rakich[10] developed an analysis and computer code which determines these metric coefficients as a function of 3-D flowfield-generated velocities. This analysis and code have been extended to include the nose-flow solution described in spherical-polar coordinates. Therefore, instead of having to initiate the integration of the equations governing the derivatives of the streamline functions [Eqs. (9), (13), and (29) in Ref. 10] at the "starting plane" for the aftbody code, initiation of the integration can now be moved upstream to the stagnation point. In the immediate neighborhood of the stagnation point, modified Newtonian pressure is used to weight, or smooth, the flowfield results over several angular mesh points. Computational "noise," which is typical around the stagnation point, is thereby reduced.

Heating Rates and Entropy-Layer Swallowing

Using the axisymmetric analogue concept,[12] the heat transfer rates to a 3-D body may be approximated by an axisymmetric boundary-layer solution by replacing the cylindrical radius, r, by the streamline metric, h. The boundary conditions at the edge of the boundary layer are obtained by double interpolation within the inviscid flowfield at the location of the boundary-layer edge. Clearly, an iteration procedure is required to establish the boundary-layer thickness, which is taken along a normal to the surface at the desired streamline location. This approach allows "swallowing" of the entropy layer by the boundary layer, since inviscid surface conditions (i.e., normal-shock expansion) no longer have to be used to establish boundary-layer edge conditions.

An estimate of the boundary-layer thickness was provided through two iterations of the following relations

$$\delta/\delta_0 = (\mu_e/\mu_{e0})/(q/q_0) \tag{1}$$

where

$$\delta_0 = 2.5\mu_0/(\{\rho\mu\}_0\{\mathrm{d}u/\mathrm{d}s\}_0)^{1/2}$$

and

$$\frac{q}{q_0} = \frac{(\{\rho\mu\}_w u_e h)(h_{as}-h_w)(.9364+.0899\{\beta\}^{1/2})}{2(\{\rho\mu\}_{w0}\{\mathrm{d}u/\mathrm{d}s\}_0\xi)^{1/2}(h_{aw}-h_w)_0} \tag{2}$$

Initial "guesses" for δ were provided by the value of δ immediately upstream, starting initially at the stagnation point with δ_0.

Table 1 Flight conditions for flowfield cases

Case	Angle of attack, deg	Altitude, kft	Velocity, kft/sec
1	41.4	246	25
2	40.2	226	21.7
3	34.5	213	19.5
4	31.8	199	16.8

Table 2 Computed sonic point locations

Case	Nose		Wing			
	PG[a]	EA[a]	PG		EA	
1	56.6[b]	20.7[b]	772[b]	(72.9)[c]	not found	
2	56.1	20.5	750	(73.8)	846	(80)
3	41.2	19.2	790	(75)	818	(78)
4	31.1	18.9	786	(75.4)	814	(78.5)

[a] PG = perfect gas, EA = equilibrium air; [b] axial distance from nose, in.; [c] meridional angle, deg.

The derivation of Eq. (1) is based on the idea that the boundary-layer thickness characterizes the boundary-layer gas-temperature gradient at a cooled surface and, therefore, is inversely proportional to the surface heat transfer rate. The heat transfer rate ratio shown in Eq. (2) has the same form as proposed by Kemp et al.[13] except that the recovery enthalpy is used in place of the total enthalpy. Results obtained using Eqs. (1) and (2) were comparable to rigorous boundary-layer calculations made using the code of Ref. 11.

Stagnation Point Heating Rates

To account for 3-D flowfield and geometry effects on the Orbiter stagnation point heating, a correction to the axisymmetric stagnation heating calculation procedure is necessary. This correction is similar to the velocity-gradient parameter introduced in 1958, by Reshotko[14] in an attempt to apply 3-D boundary-layer equations to a general 3-D stagnation point. This parameter can be expressed as

$$K = \left(\frac{\partial w}{\partial n}\right) \Big/ \left(\frac{\partial u}{\partial s}\right) \tag{3}$$

where $(\partial u/\partial s)$ and $(\partial w/\partial n)$ are streamwise and crosswise velocity gradients. For Newtonian flow, K would be equal to Rs/Rn, where Rs and Rn are the streamwise and crosswise radii of curvature. However, since the stagnation point is in a relatively large subsonic region (see Table 2), local geometric radii of curvature may not properly define the local velocity gradient when the local radii of curvature change significantly. Therefore, more exact flowfield based velocity gradients were used in this study, since the radii of curvature change rapidly (from a spherical segment to a cubic curve) in the stagnation region. Specifically, the effective 3-D velocity gradient was taken to be the average of the two principal velocity gradients at the stagnation point. Therefore, the 3-D stagnation heating rates, q_s, were estimated by using a correction factor with the 2-D stagnation point heating rate, q_0, as shown in the following expression.

$$q_s = F \cdot q_0 \tag{4}$$

and

$$F=\left[\frac{(K+1)}{2}\cdot\frac{(\partial u/\partial s)}{(\partial u/\partial s)_0}\right]^{1/2} \tag{5}$$

where the 2-D velocity gradient $(\partial u/\partial s)_0$ is approximated by modified Newtonian theory.

The two principal velocity gradients are obtained using a 3-D time-dependent code.[7] This simple "3-D" stagnation point correction was compared with an existing "3-D" stagnation heating correlation presented by DeJarnette and Hamilton[15] which was based on the earlier works of Lees,[16] Reshotko,[14] and Cohen.[17] The heating rates obtained using Eq. (29) in Ref. 15, with thermodynamic and transport properties calculated using the boundary-layer code of Ref. 11 and velocity gradients computed from the current inviscid flowfields, agreed with the current predictions to within 0.9 percent for all four equilibrium air cases.

Results and Discussion

Results of flowfield and heating rate predictions made around much of the Orbiter windward surface at the second trajectory point used in this study (indicated as "Case 2" in Table 1) will be described in detail in this section. Generally, the trends in the variations of heating and boundary-layer edge conditions caused by changing flowfield parameters apply to other cases as well. Limited comparisons between the present flowfield results and 2-D flowfield-based extrapolations of wind-tunnel data[2] have also been made.

In addition, changes in heating rates with velocity, which reflect results obtained at all four flight cases, have been presented for three body points which typify the challenging and complex nature of the Orbiter 3-D flowfield. These points are located in the nose stagnation region, and the fuselage centerline and wing-root region near the leading edge for $x=0.62\ L$ (designated at points A, B, and C, respectively, in Fig. 1a).

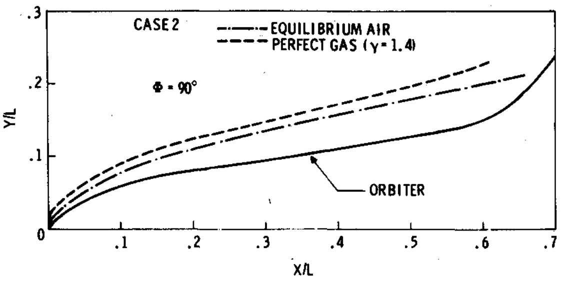

a) PLANFORM

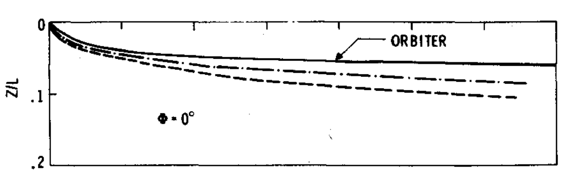

b) PROFILE

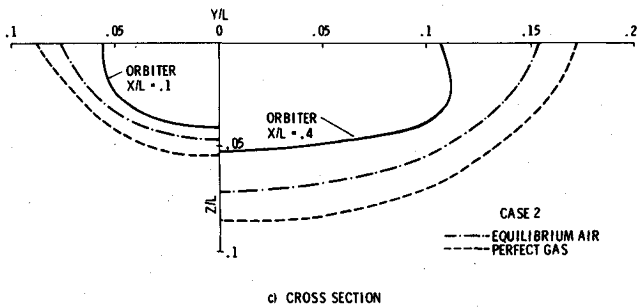

c) CROSS SECTION

Fig. 2 Influence of gas chemistry on Orbiter shock shape.

Results for Case 2

Presentations of flowfield predictions will be limited to the windward surface of the Orbiter from the nose to an axial location of approximately $x=0.7\ L$. This is due to the current limitation in the inviscid computation method which requires the local flow to be supersonic in the axial direction. The detailed locations of the points where the flow is locally transonic are shown in Table 2.

Presentations of shock shape, surface pressure, and heating rate predictions for two gas models (equilibrium air and a perfect gas) and two entropy conditions (normal-shock entropy and entropy determined within the inviscid flowfield through entropy-layer swallowing considerations) are shown both along the windward centerline and in a circumferential, or lateral manner, at selected axial stations. Presentations of boundary-layer edge conditions will be limited to the centerline.

Shock Geometry

Figure 2 illustrates the effect of gas chemistry on the shape and location of the Orbiter shock layer. As expected, the equilibrium air shock-layer thickness is from 60 to 70 percent of the perfect gas thickness. The actual shock wave will be somewhere between these two shocks, since the actual flow is governed by finite-rate-chemistry[5] at these flight conditions. However, a reasonable definition of the shock location, particularly the approximate location of the fuselage-shock/wing-shock interaction can be obtained using these two limits. The relative thicknesses of the shock layer over most of the windward surface is illustrated for the centerline in Fig. 2b, and for two cross-sections located at $x=0.1\ L$ and $0.4\ L$ in Fig. 2c.

Centerline Pressure and Heating

Figure 3 characterizes the pressure distribution along the centerline for several different prediction methods. Relative to modified Newtonian theory, the present flowfield methods predict an overexpansion near the nose region ($x=0.02\ L$ to $0.08\ L$) and a recompression after $x=0.2\ L$ for both equilibrium air and perfect gas. Trangent-cone-based data extrapolations also predict a recompression near the same region. However, very little overexpansion is predicted using these data extrapolation methods.

Figure 4 indicates the sensitivity of laminar heating predictions to changes in entropy and gas chemistry. These predictions were made using the pressures shown in Fig. 3 for a surface temperature of 2000°R. In general, the effects of entropy-layer swallowing appear almost immediately (at $x=0.01\ L$, perhaps due to the large angle of attack and high crossflow). The heating predictions are approximately 50 percent higher than the normal-shock entropy predictions made using the same pressures. On the other hand, changing gas models increase the heating predictions by roughly 30

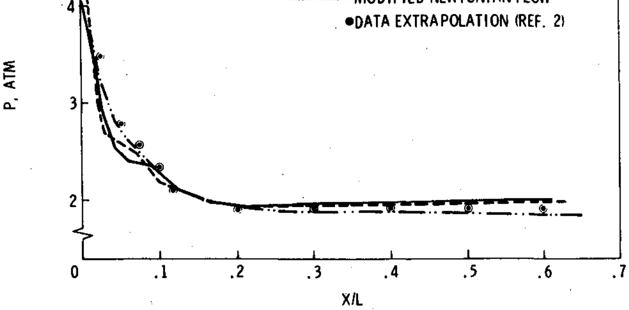

Fig. 3 Effects of gas chemistry on centerline pressure.

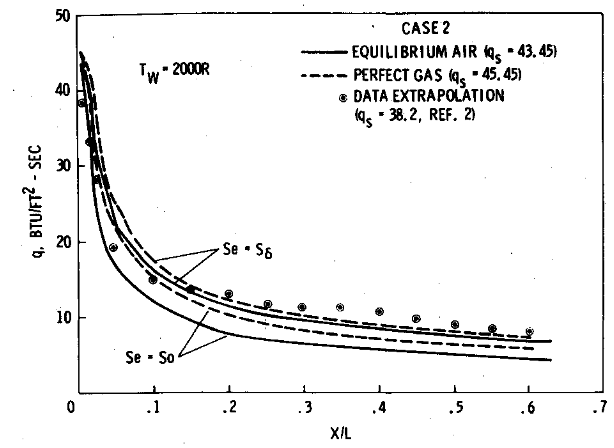

Fig. 4 Effects of gas chemistry and entropy-layer swallowing on centerline heating.

percent higher than the equilibrium air results using normal-shock entropy and up to 15 percent for the entropy-layer swallowing case. Therefore, for the most realistic case, whch considers entropy-layer swallowing, the gas model plays a secondary role in establishing the heating rates (remark limited to fully catalytic surfaces).

Figure 4 also presents current Orbiter design data, which reflect hypersonic wind-tunnel data which have been adjusted or scaled for high velocity and equilibrium air chemistry.[2] These data generally agree with the equilibrium air, normal-shock heating predictions near the nose. However, this may be due to the influence of the wind-tunnel data (which has a relatively thick entropy layer near the nose that produces normal-shock-like entropy edge conditions[3]) on the calibration or "three-dimensionalization" of the two-dimensional-based flowfield scaling method used in Ref. 2. Other effects, such as differences in the wind-tunnel model geometry and the analytical flowfield Orbiter geometry (see cross-sections in Fig. 1c) could contribute to these differences near the nose where geometry curvature is important. In addition, beyond $x = 0.13\,L$, the data extrapolations are above all of the predictions. Recalling that the predicted pressures were near the extrapolated pressures in this region suggests that the entropy produced from the tangent-cone-based flow model is lower than the three-dimensional flowfield model. (This trend will again be noted when the boundary-layer edge conditions are discussed in the next section.)

Boundary-Layer Edge Conditions

Figure 5a illustrates the sensitivity of the predicted boundary-layer thicknesses to the flow parameters used in this study. The perfect gas boundary-layer thicknesses are up to 60 percent greater than the equilibrium air calculations for both entropy edge conditions. For both gas models, the predictions made using normal-shock entropy were roughly 60 percent higher than the entropy-layer swallowing predictions. The reason for this will become clearer when the edge Reynolds number is examined for each of these cases.

Figure 5a also relates the boundary-layer thickness to the equilibrium air inviscid-entropy-layer thickness for $x = 0.5\,L$. For the more realistic case which considers entropy-layer swallowing, the equilibrium air boundary layer has "swallowed" approximately 50 percent of the entropy layer. This effect will produce edge conditions which are between normal-shock expansion and tangent-cone results as will be shown in the figure covering edge Mach numbers.

Figure 5b shows that the equilibrium air values of Re_x are reduced approximately 60 percent due to normal-shock entropy edge conditions and reduced slightly more due to gas model changes. Certainly changes in entropy-layer swallowing and gas models experienced in scaling from wind tunnel to flight could have a large influence on boundary-layer transition correlations based on Re_x alone, if not properly scaled to account for these changes.

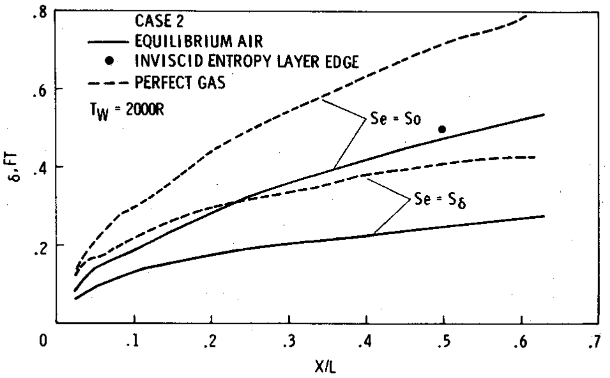

a) BOUNDARY LAYER THICKNESS

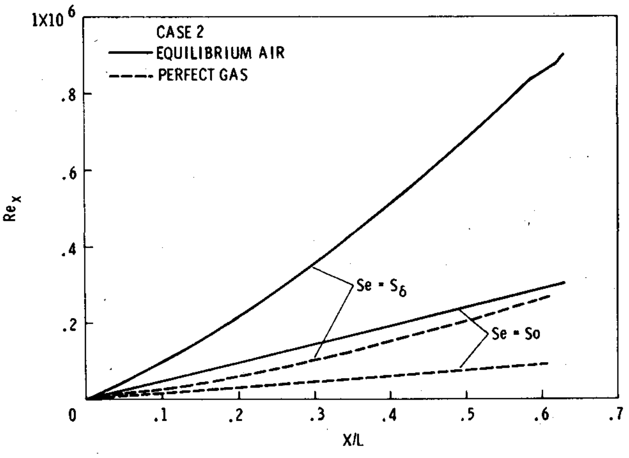

b) REYNOLDS NUMBER

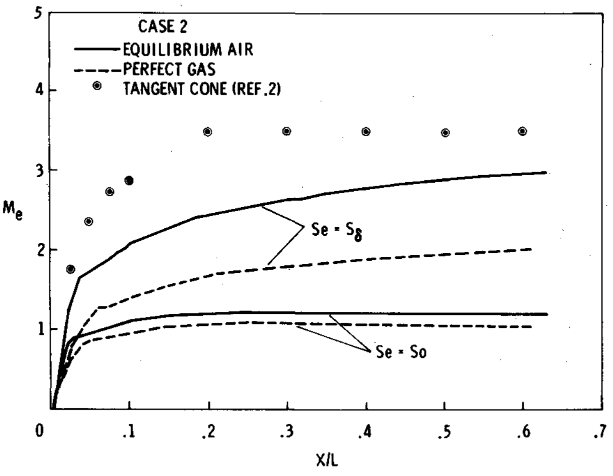

c) MACH NUMBER

Fig. 5 Effects of gas chemistry and entropy-layer swallowing on centerline boundary-layer edge conditions.

Figure 5c illustrates the strong influence of the entropy on edge Mach number distributions. Using a normal-shock expansion, the flow is barely supersonic ($M_e \simeq 1.2$) along most of the centerline; whereas, for swallowed-entropy-layer edge conditions, the Mach number approaches three at $x = 0.6\,L$. Corresponding tangent-cone-based predictions[2] show a much faster rise in Mach number near the nose and approaches 3.5 near $x = 0.2\,L$.

Lateral Pressure and Heating Distributions

Figure 6a shows the lateral distribution of normalized pressure, p/p_0, plotted versus normalized lateral length, y/B. (The reader is encouraged to refer to the Orbiter cross sections shown in Fig. 1c and planform shown in Fig. 1a to help relate

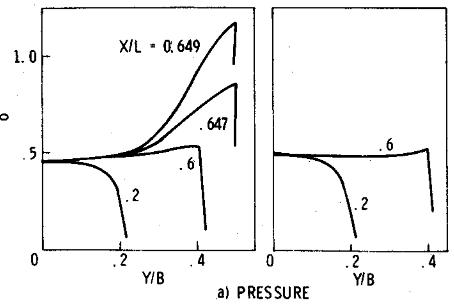

a) PRESSURE

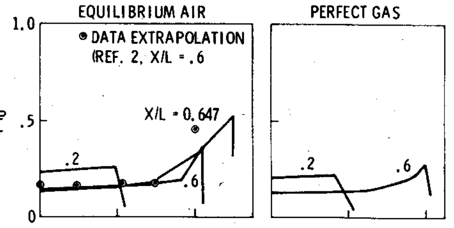

b) HEATING

Fig. 6 Lateral distribution of pressure and heating.

these distributions to changes in cross-sectional geometry and leading edge sweep.) For the axial stations shown, the lateral distributions of pressure change very little with gas chemistry. (Stations beyond $x \simeq 0.6\,L$ were not shown for the perfect gas case since, as previously indicated, the inviscid computation was terminated due to low axial Mach numbers.) In general, near the nose, the pressure decreases smoothly when moving laterally from the centerline to the "chine" line or fuselage leading edge. Further down the vehicle near the location of the fuselage-wing junction or wing-root area ($x \simeq 0.6\,L$), the wing begins to influence the lateral pressure distribution as shown in Fig. 6a. Between $x = 0.6\,L$ and $0.649\,L$, the "chine" sweep changes from approximately 80 to 45 deg. Hence, this geometry change decelerates or turns the local supersonic flow and forms an imbedded shock wave. This is clearly shown in Fig. 6a, since the local pressures have exceeded the stagnation point normal-shock pressures; i.e., $p/p_0 > 1.0$.

Figure 6b illustrates similar lateral distributions for normalized heating, q/q_0 (q_0 is the stagnation-point heat transfer rate for a sphere with the Orbiter nose cap radius; i.e., $R = 28.33$ in. and exposed to the same freestream flow as the stagnation point). The perfect gas and equilibrium distributions are generally similar for the stations shown, although the equilibrium heating is higher at the wing-root chine ($x \simeq 0.6\,L$). Extrapolated data from the current Orbiter design analysis[2] are similarly normalized and shown for comparison at $x = 0.6\,L$. The distributions are quite similar. Near the "chine," the present predictions are lower than the data extrapolations. However, due to the relatively coarse streamline spacing used for this region, the peak heating predictions were not necessarily established. Except at the actual chine location, the real and analytical Orbiter geometries are comparable for this axial station (see Fig. 1c). Therefore, this agreement reinforces the current data extrapolation methods used for the Orbiter in this region.

Heating Versus Entry Velocity

Flowfield results from all four flight cases described in Table 1 have been assembled to help characterize the heating to several body points as the Orbiter passes through the peak laminar heating regime during entry. These points are the nose stagnation point, the fuselage centerline at $x = 0.62\,L$, and the wing root at $x = 0.62\,L$ and $y = 0.16\,L$ (or $y = 0.44\,B$) which is downwind of where the wing reaches a sweep of 45 deg.

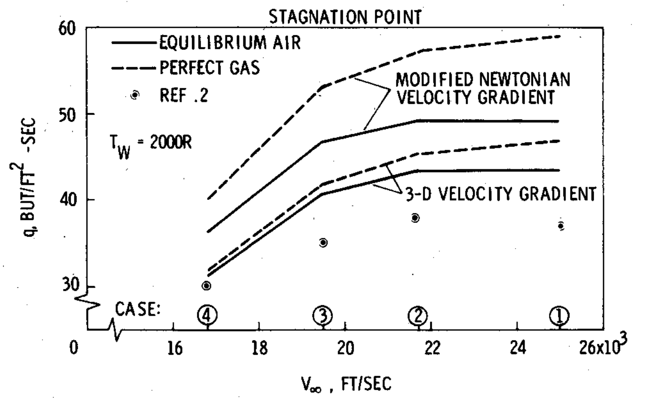

Fig. 7 Influence of gas chemistry and velocity gradient on stagnation-point heating.

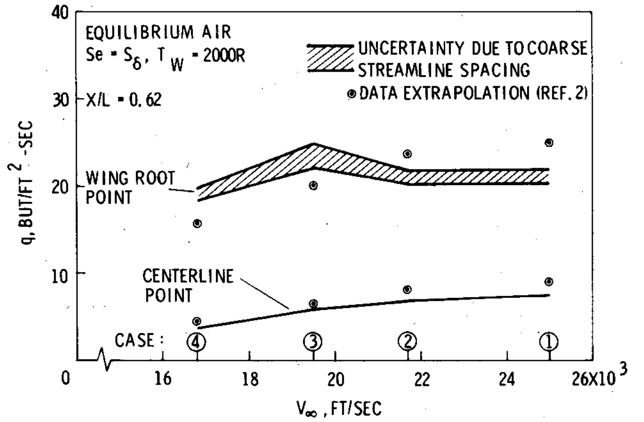

Fig. 8 Equilibrium air heat transfer to centerline and wing-root points.

The behavior of the stagnation-point heating is frequently characterized as a sphere with some effective radius, depending on the angle of attack. However, using the methods described in the Analysis Section, the stagnation-point heating rates are influenced rather significantly by the principle velocity gradients in the streamwise and crossflow directions, which reflect the three-dimensionality of the stagnation point region. Even though the current analytical description of the Orbiter used a 28.33-in. radius spherical segment to describe the first 10 in. of the Orbiter, the location of the subsonic flow region near the nose extended well beyond this spherical segment. (Refer to Table 2 for the actual size of the subsonic region.) Therefore, the flow in the stagnation-point region is actually influenced by a much larger effective body with a larger effective radius of curvature than the actual geometry. As indicated in Table 2, the subsonic zone size will change with the angle of attack and gas chemistry. Therefore, the effective radius is influenced by both of these factors.

To illustrate this point, Fig. 7 shows the stagnation-point heating from predictions made using both equilibrium air and a perfect gas. These predictions were made using both conventional modified-Newtonian-flow velocity gradients and 3-D flowfield velocity gradients obtained from the current inviscid flowfields. Using the modified-Newtonian velocity gradients (which are appropriate for axisymmetric bodies at high Mach numbers), the perfect gas heating rates are 20 percent higher than the equilibrium air values for the higher velocities. As expected, the predictions converged at the lower velocities, where the flow enthalpies are reduced by more than 50 percent. Similarly, using 3-D flowfield velocity gradients to form effective stagnation-point velocity gradients appears to reduce the differences between the perfect gas and equilibrium air predictions to approximately eight percent at the higher freestream velocities. This effect also causes the two predictions to converge more rapidly at the lower velocities. The reduction in the perfect gas heating due to 3-D velocity gradients is typically 25 percent, whereas, the equilibrium air reductions range from 13 to 16 percent.

Also shown in Fig. 7 are Fay and Riddell[18] based extrapolations[2] of wind-tunnel stagnation point data for these same flight conditions. These predictions were made using a Lewis number of 1.0, which eliminated the contribution of dissociated gas energy to the surface heat transfer. Approximately 50 to 60 percent of the flow energy is in dissociation at the higher velocities. This energy could increase the heating by as much as 11 percent if a Lewis number of 1.4 were used in these predictions. The current predictions and the data extrapolations of Ref. 2 are in good agreement at the lower velocity, where the contribution of the dissociated-gas energy is small. This should be expected, since the Lewis number no longer contributes significantly to the heating calculations at these conditions.

Figure 8 shows the heating predictions versus velocity for the centerline and wing-root region located at $x=0.62\ L$ (points B and C in Fig. 1a). As expected, the laminar heating to the centerline point decreased as the velocity (and angle of attack) decreased. This same trend can also be predicted with a tangent-cone-based data extrapolation method.[2] However, these data predictions, which are also in Fig. 8, are roughly 16 to 20 percent higher than the current predictions.

Figure 8 also characterizes the wing-root heating through this phase of the Orbiter entry trajectory. Note, an uncertainty band of roughly 10 percent has been placed on the predictions due to the coarseness of the streamline pattern near this region. Thus, the actual peak heating predictions may not have been established. These predictions do, however, represent the trend of the wing-root heating with velocity and angle of attack. The increased heating predicted for Case 3 is due partly to a large reduction in angle of attack relative to Cases 1 and 2 (~41 to 34.5 degrees). Apparently, this reduction in angle of attack exposed the wing root to a more severe local environment, which offset the anticipated reduction in heating caused by the reduced freestream velocity (as indicated by the centerline point).

Concluding Remarks

Using exact 3-D flowfield codes, 2-D boundary-layer analyses, and approximate heating correlations, in conjunction with the axisymmetric analogue concept, predictions of the Orbiter aerothermodynamic environment were made for four points selected from the current Orbiter design trajectory. These predictions included shock shapes, pressure, heating rates, and selected boundary-layer edge condtions. A relatively simple "entropy-layer swallowing" concept was developed for these 3-D flowfields and used to establish realistic boundary-layer edge conditions. In addition, due to the highly nonaxisymmetric (i.e., highly 3-D) flow in the stagnation-point region, an effective "3-D" velocity gradient expression was developed and used to correct (lower) the axisymmetric stagnation-point heating predictions. All predictions made using these codes considered two gas models (equilibrium and perfect air) in an effort to provide a rough assessment of the effects of finite-rate-chemistry on these results. This approach also provides a good indication of the differences that exist in the inviscid portion of the flowfield at hypersonic wind-tunnel and flight conditions.

Predictions made using these flowfield concepts were compared to 1) normal-shock expansion results (i.e., predictions made without considering "entropy layer swallowing") and 2) current Orbiter design predictions based on scaled wind tunnel data. These comparisons revealed the following:

Pressure Results

1) The flowfield results show a relatively strong overexpansion and recompression near the nose.

2) Embedded pockets of high pressure flow ($p/p_0>1$) exist in the multi-shock region near the root of the wing leading edge.

3) Gas chemistry has a small effect on the pressure predictions.

Heating Results

1) Comparable heating can be predicted using either exact boundary-layer analyses or relatively simple heating correlations.

2) Heating predictions downstream of $x=0.04\ L$ were strongly dependent on entropy-layer swallowing.

3) Gas chemistry had a relatively small influence on heating predictions with entropy layer swallowing and fully catalytic surfaces.

Boundary-Layer Edge Conditions

1) Entropy-layer swallowing strongly influences edge conditions.

2) Gas chemistry affects edge conditions significantly, but less than entropy-layer swallowing.

3) Edge-condition boundary-layer-transition parameters are strongly influenced by both entropy-layer swallowing and gas chemistry.

Generally, the current Orbiter design methods used to predict laminar heating provide predominantly conservative results relative to these flowfield predictions. An exception to this is in the Orbiter nose region. However, these flowfield results are current being used to help "calibrate" the design-prediction methods over the range of flight conditions considered in this study.

Acknowledgment

The authors acknowledge the valuable assistance provided by John Rakich and Walter Reinhardt of NASA Ames Research Center for helping to implement, modify, and execute those codes developed at Ames.

References

[1] Goodrich, W. D., Li, C. P., Houston, C. K., Meyers, R. M., and Olmedo, L., "Scaling of Orbiter Aerothermodynamic Data Through Numerical Flow Field Simulations," NASA, SP-347, March 1975.

[2] "Space Shuttle Orbiter Entry Aerodynamic Heating Data Book," Rockwell International, Space Division, Downey, Calif., SD73-SH-0184B, Feb. 1976.

[3] Martindale, W. R. and Carter, L. D., "Flow-Field Measurements in the Windward Surface Shock Layer of Space Shuttle Orbiter Configurations at Mach Number 8," AEDC-TR-75-5, Jan. 1975.

[4] Martindale, W. R., "Test Results from the NASA/Rockwell International Space Shuttle Test (OH4B) Conducted in the AEDC-VKF Tunnel B ," AEDC-DR-74-8, Jan. 1974.

[5] Rakich, J. V. and Lanfranco, M., J., "Numerical Computations of Space Shuttle Heating and Surface Streamlines," AIAA Paper 76-464, July 1976.

[6] Adams, J. C. Jr., Martindale, W. R., Mayne, A. W. Jr., and Marchand, E. O., "Real Gas Effects on Hypersonic Laminar Boundary-Layer Parameters Including Effects of Entropy-Layer Swallowing," AIAA Paper 76-358, July 1976.

[7] Li, C. P., "A Numerical Study of Laminar Flow Separation on Blunt Flared Cones at Angle of Attack," AIAA Paper 74-585, June 1974.

[8] Kutler, P., Reinhardt, W. A., and Warning, R. F., "Multishocked Three-Dimensional Supersonic Flow Fields with Real Gas Effects," *AIAA Journal*, Vol. 11, May 1973, pp. 657-664.

[9] Kutler, P., Warning, R. F., and Lomax, H., "Computations of Space Shuttle Flow Fields Using Noncentered Finite Difference Schemes," *AIAA Journal*, Vol. 11, Feb. 1973, pp. 196-204.

[10] Rakich, J. V. and Mateer, G. G., "Calculation of Metric Coefficients for Streamline Coordinates," *AIAA Journal*, Vol. 10, Nov. 1972, pp. 1538-1540.

[11] Tong, H., Buckingham, A. C., and Curry, D. M., "Computational Procedure for Evaluation of Space Shuttle TPS Requirements," AIAA Paper 74-518, June 1974.

[12] DeJarnette, F. R. and Davis, R. M., "A Simplified Method for Calculating Laminar Heat Transfer Over Bodies at Angle of Attack," NASA TN D-4720, 1968.

[13] Kemp, N.H., Rose, P.H., and Detra, R.W., "Laminar Heat Transfer Around Blunt Bodies in Dissociated Air," *Journal of Aero/Space Science*, Vol. 26, July 1959, pp. 421-430.

[14] Rehotko, E., "Heat Transfer to a General Three-Dimensional Stagnation Point," *Jet Propulsion*, Vol. 28, Jan. 1958, pp. 58-60.

[15] DeJarnette, F. R. and Hamilton, H. H., "Inviscid Surface Streamlines and Heat Transfer on Shuttle-Type Configurations," *Journal of Spacecraft and Rockets*, Vol. 10, May 1973, pp. 314-321.

[16] Lees, L., "Laminar Heat Transfer over Blunt-Nosed Bodies at Hypersonic Flight Speeds," *Jet Propulsion*, Vol. 26, April 1956, pp. 259-269.

[17] Cohen, N. B., "Boundary-Layer Similar Solutions and Correlation Equations for Laminar Heat-Transfer Distribution in Equilibrium Air at Velocities Up to 41,000 Feet Per Second," NASA TR R-118, 1961.

[18] Fay, J. A. and Riddell, F. R., "Theory of Stagnation Point Heat Transfer in Dissociated Air," *Journal of Aero/Space Science*, Vol. 25, Feb. 1958, pp. 73-85, 121.

From the AIAA Progress in Astronautics and Aeronautics Series

SPACECRAFT CHARGING BY MAGNETOSPHERIC PLASMAS—v. 47

Edited by Alan Rosen, TRW, Inc.

Spacecraft charging by magnetospheric plasma is a recently identified space hazard that can virtually destroy a spacecraft in Earth orbit or a space probe in extra terrestrial flight by leading to sudden high-current electrical discharges during flight. The most prominent physical consequences of such pulse discharges are electromagnetic induction currents in various onboard circuit elements and resulting malfunctions of some of them; other consequences include actual material degradation of components, reducing their effectiveness or making them inoperative.

The problem of eliminating this type of hazard has prompted the development of a specialized field of research into the possible interactions between a spacecraft and the charged planetary and interplanetary mediums through which its path takes it. Involved are the physics of the ionized space medium, the processes that lead to potential build-up on the spacecraft, the various mechanisms of charge leakage that work to reduce the build-up, and some complex electronic mechanisms in conductors and insulators, and particularly at surfaces exposed to vacuum and to radiation.

As a result, the research that started several years ago with the immediate engineering goal of eliminating arcing caused by flight through the charged plasma around Earth has led to a much deeper study of the physics of the planetary plasma, the nature of electromagnetic interaction, and the electronic processes in currents flowing through various solid media. The results of this research have a bearing, therefore, on diverse fields of physics and astrophysics, as well as on the engineering design of spacecraft.

304 pp., 6 x 9, illus. $16.00 Mem. $28.00 List

TO ORDER WRITE: Publications Dept., AIAA, 1290 Avenue of the Americas, New York, N. Y. 10019